Kinetic trajectory decoding using motor cortical ensembles

Andrew H. Fagg[1], Greg Ojakangas[2], Lee E. Miller[3], & Nicholas G. Hatsopoulos[4]

[1]*School of Computer Science, University of Oklahoma, Norman, OK*

[2]*Dept. of Physics, Drury University*

[3]*Dept. of Physiology, Northwestern University, Chicago, IL, 60611*

[4]*Dept. of Organismal Biology and Anatomy and Committee on Computational Neuroscience, University of Chicago, Chicago, IL 60637*

The first two authors contributed equally to this work.

Correspondence and requests for reprints to Nicholas G. Hatsopoulos, Dept. of Organismal Biology and Anatomy, University of Chicago, Chicago, IL 60637. Phone: (773)702-5594. Fax: (773)702-0037. E-mail: nicho@uchicago.edu.

Running Head: Kinetic Decoding using Motor Cortical Ensembles

Key words: torque decoding, primary motor cortex, multi-electrode recording

Total number of words: 7014

Abstract

Although most brain-machine interface (BMI) studies have focused on decoding kinematic parameters of motion such as hand position and velocity, it is known that motor cortical activity also correlates with kinetic signals, including active hand force and joint torque. Here, we attempted to reconstruct torque trajectories of the shoulder and elbow joints from the activity of simultaneously recorded units in primary motor cortex (MI) as monkeys (*Macaca Mulatta*) made reaching movements in the horizontal plane. Using a linear filter decoding approach that considers the history of neuronal activity up to one second in the past, we found reconstruction performance nearly equal to that of Cartesian hand position and velocity, despite the considerably greater bandwidth of the torque signals. Moreover, the addition of delayed position and velocity feedback to the decoder generated consistently better torque reconstructions, suggesting that simple limb-state feedback may be useful to optimize BMI performance. These results may be relevant for BMI applications that require controlling devices with inherent, physical dynamics or applying forces to the environment.

Introduction

The early pioneering electrophysiological experiments of Evarts suggested that single pyramidal tract MI neurons encode primarily the force (or its temporal derivative) applied by the limb rather than movement per se [1]. A dichotomy is often drawn between this early work, and that of Georgopoulos, who showed a striking relation between MI discharge and the direction of hand movement [2]. Numerous subsequent studies have provided evidence that MI encodes a variety of kinetic and kinematic signals, including joint torque and hand force [3-9], position [10, 11], velocity [12], direction of hand movement [2, 13]. Nonetheless, virtually all real-time brain-machine interfaces have focused only on kinematic variables [14-17].

However, an early pioneering study predicted wrist joint torque from a small number of motor cortical units [18]. More recently, a study demonstrated grip force decoded from motor cortical ensembles [19]. Moreover, EMG activity can be reconstructed from groups of MI neurons [20-23]. These recent decoding results, as well as the earlier force encoding studies, suggest that it should be possible to control a dynamical limb by predicting the torques generated by the shoulder and elbow joints during reaching.

We recorded simultaneously from multiple single units in MI using chronically implanted electrode arrays while monkeys performed a random-target pursuit task. This task generated a rich variety of trajectories with varied curvatures, velocities, and positions. We used linear regression techniques to predict shoulder and elbow torque from the activity of the recorded neurons, which we compared to the corresponding kinematic predictions.

Methods

Behavioral Tasks and Kinematics

Three monkeys (*Macaca Mulatta*) were used in these experiments. Each monkey's upper arm was abducted 90 degrees and rested on cushioned troughs secured to links of a two-joint robotic arm (KINARM system; Figure 1) [24]. The robotic arm constrained movement to a horizontal plane, but did not limit movement within this plane. The cursor and a sequence of targets were projected on a horizontal screen immediately above the monkey's arm. At the beginning of a trial, a target appeared at a random location in the workspace and the monkey was required to move to it. As soon as the cursor reached the target, the target disappeared and was replaced by a new one in a random location. After reaching the seventh target, the monkey was

rewarded with a drop of water. The monkeys typically executed 400 to 800 successful trials in the course of a 1 to 1.5 hours recording session.

The shoulder and elbow joint angles were sampled at 500 Hz using the robotic arm's motor encoders and acquired along with neural data. The *X* and *Y* positions of the hand were computed by transforming the joint angles into Cartesian end-points using the standard forward kinematics equations for a two-joint arm [25]. The lengths of the upper arm and forearm of the monkey were estimated using x-ray images of the humerus and the distance from the elbow joint to the palm, respectively.

Electrophysiology

Silicon-based electrode arrays (Cyberkinetics Neurotechnology Systems, Inc., MA) composed of 100 electrodes (1.0 mm electrode length; 400 μm inter-electrode separation) were implanted in the arm area of primary motor cortex (MI) contralateral to the moving arm on the precentral gyrus of each monkey. Surgical implantation was performed using Isoflurane. During a recording session, signals from up to 96 electrodes were amplified (gain, 5000) and digitized (14-bit) at 30 kHz per channel using a Cerebus acquisition system (Cyberkinetics Neurotechnology Systems, Inc., MA). Waveforms that crossed a threshold were stored and spike-sorted using Offline Sorter (Plexon, Inc., Dallas, TX). Inter-spike interval histograms were computed to verify single-unit isolation by ensuring that less than 0.05% of waveforms possessed an inter-spike interval less than 1.6 ms. Signal-to-noise ratios were defined as the difference in mean peak-to-trough voltage of the waveforms divided by the mean (over all 48 time samples of the waveform) standard deviation of the waveforms. All isolated single units used in this study possessed signal-to-noise ratios of 4:1 or higher. Two data sets were analyzed from each of three animals, BO, RJ, and RS (see table 1). A data set is defined as all simultaneously recorded neural and kinematic data collected in one recording session. Each data set contained between 31 and 99 simultaneously recorded units from MI. The ensembles consisted of "randomly" selected units from MI except for a possible bias for neurons with large cell bodies that would generate higher signal-to-noise ratios. All of the surgical and behavioral procedures were approved by the University of Chicago's IACUC and conform to the principles outlined in the Guide for the Care and Use of Laboratory Animals (NIH publication no. 86-23, revised 1985).

Equations of motion

The KINARM exoskeletal robot is composed of five segments, labeled L1 through L5 in Figure 1. As illustrated, the monkey's shoulder and elbow joints are coincident with the proximal pivot axes of segments 1 and 2. Segments 1 and 4 remain parallel at all times, as do segments 3 and 5. Segment 5 is rigidly attached to segment 2 at an angle of 155 degrees. Torque motors 1 and 2, not actively employed in this study, are attached by belts to segments 1 and 3, and thus contribute passively to rotational inertias. Relevant arm segment inertias for the monkeys were added to those of KINARM segments 1 and 2 (with which they were coincident during valid trials). The arm segment inertias were estimated using the approach of Cheng and Scott [26] and were based on each monkey's body mass on the day the data set was recorded (see Appendix A for details). The equations of motion for the combined system consisting of the monkey's arm and the associated moving components of the KINARM were derived in a standard manner using Hamilton's principle applied to the Lagrangian for the system [27]. Expressed in terms of the planar shoulder and elbow angles θ_1 and θ_2 (see Figure 1), the equations are as follows:

$$\tau_1 = A(\theta_2)\ddot{\theta}_1 + B(\theta_2)\ddot{\theta}_2 - C(\theta_2)(2\dot{\theta}_1\dot{\theta}_2 + \dot{\theta}_2^{\,2}), \text{ and} \tag{1a}$$

$$\tau_2 = B(\theta_2)\ddot{\theta}_1 + D\ddot{\theta}_2 + C(\theta_2)\dot{\theta}_1^{\,2}, \tag{1b}$$

where:

$$A(\theta_2) = \sum_{i=1}^{5} I_i + I_{m1} + I_{m2} + M_2 L_1^2 + M_4 L_3^2 + 2g(\theta_2), \tag{2a}$$

$$B(\theta_2) = D + g(\theta_2), \tag{2b}$$

$$C(\theta_2) = M_2 L_1(\overline{x_2}\sin\theta_2 + \overline{y_2}\cos\theta_2) + M_4 L_3(\overline{x_4}\sin(\theta_2 - \Delta) - \overline{y_4}\cos(\theta_2 - \Delta)), \tag{2c}$$

$$g(\theta_2) = M_2 L_1(\overline{x_2}\cos\theta_2 - \overline{y_2}\sin\theta_2) + M_4 L_3(\overline{x_4}\cos(\theta_2 - \Delta) + \overline{y_4}\sin(\theta_2 - \Delta)), \text{ and} \tag{2d}$$

$$D = I_2 + I_3 + I_5 + I_{m2} + M_4 L_3^2. \tag{2e}$$

In the above equations, τ_1 and τ_2 represent the net torque applied to the shoulder and elbow in order to account for the observed motion. The torques are due not only to actively generated muscle forces, but also to other viscoelastic effects that result from the musculoskeletal system and the KINARM. I_i, M_i and L_i are the rotational inertias (with respect to the proximal pivots), masses, and inter-joint lengths of the numbered segments, $(\overline{x}_i, \overline{y}_i)$ is the center-of-mass location

of the i_{th} segment in a right-handed, proximal-pivot-centered coordinate system with the x-axis directed along the length of the segment, and I_{Mi} are the effective rotational inertias for the shoulder- and elbow-torque motors.

Spectral content and filtering of signals

Because the differentiation required to estimate angular velocity and acceleration significantly amplifies high frequency noise, the position signals were digitally low-pass filtered below 6 Hz with a 3-pole Butterworth filter. The filter was applied in both the forward and reverse directions to eliminate phase distortions [28], resulting in a composite 6-pole filter. As anticipated, there remained significantly more movement-related power at frequencies above 0.5 Hz in the torque signals than in the position signals. The performance of the torque predictions was dependent on the degree of filtering: predictions improved as the filter corner was decreased from 20 to 4Hz. Presumably this was the result of the elimination of higher frequency, differentiation noise in the torque signals. A corresponding decrease did not occur for the position predictions, as there was very little power in the original signals above several Hz. As the filter corner approached 4 Hz, there would also have been some impact on movement-related (< 5 Hz) frequencies. Although the ideal corner frequency for filtering remains unclear, we chose 6 Hz for the remainder of the analysis.

One form of torque decoder that we explored makes use of joint position and velocity as additional inputs to the decoder. Under these conditions, position was smoothed with a realizable (causal) 1 pole, 6 Hz Butterworth filter prior to differentiation. In practice, this filter induced an approximate delay of 50 ms in the position and velocity signals.

Analysis

Reconstructions of Cartesian end-point position and velocity, and shoulder and elbow torque were computed from the neural data using separate, linear models. Predictions at time index j (denoted p_j), were obtained from the linear weighted discharge of multiple neurons at multiple time points in the past (this is referred to as a linear filter decoder). The predicted quantity, denoted $\hat{p}_j$, was computed as follows:

$$\hat{p}_j = f_0 + \sum_{n=1}^{N} \sum_{i=1}^{L} r_{j-i}^{n} f_i^{n}, \qquad (3)$$

where N is the number of simultaneously recorded neurons, L is the filter length in number of time bins, r_j^n is the discharge of neuron n at time index j, and the f_i^n denote the set of filter coefficients. The discharge of an individual neuron at one time point was estimated using the number of spikes evoked within a time bin of length B. N ranged from 31 to 99 neurons (depending upon the data set). L was set to 20, and B was set to 50 ms, resulting in a filter length of one second. The values of the linear filter coefficients were selected so as to minimize the sum squared difference between the predicted quantities, $\hat{p}_j$, and the actual quantities, p_j, using a Moore-Penrose pseudo-inverse method [29, 30].

The performance of a given model was assessed using a test data set that was sampled independently of the data used to construct the model. In order to facilitate a comparison between different models, and, in particular, between different predicted variables, performance was measured in terms of the *fraction of variance accounted for* (FVAF) by the model [30]:

$$FVAF = 1 - \frac{\sum_{j=1}^{M} \left(p_j - \hat{p}_j \right)^2}{\sum_{j=1}^{M} \left(p_j - \bar{p} \right)^2}, \tag{4}$$

where M is the number of samples in the data set, $\bar{p}$ is the mean over the actual quantities (for the test set), and $-\infty \leq FVAF \leq 1$. Note this measure's similarity to the R-squared statistic. The difference is that this measure reaches unity only with an exact match between the observation and the prediction, rather than with only a perfect linear correlation. This is a property that becomes critical once the predicted motion is used to determine the actual motion of a robot arm.

Each model was assessed using a twenty-fold cross-validation approach. Here, the data set was partitioned into 20 independent "folds" [31-33], each consisting of data from an equal number of trials. For each fold, a separate model was constructed, leaving that fold out for use as *test data* and using eighteen of the remaining folds as training data. The test data fold was used to compare the performance across different model forms. The one remaining fold was used under certain conditions as a *validation data set*: model performance with respect to this data set was used to select some model parameters (e.g., proprioceptive feedback delay), before evaluating the model for comparison with other model forms using the test data. This approach

eliminates any bias that may be introduced by selecting the model parameters on the basis of the test set performance [32].

In practice, the FVAF measures from a set of N models generally were not distributed normally, precluding the use of a t-test for detecting significant differences in mean model performance. These situations were detected using a Shapiro-Wilk test [34]. When applicable, bootstrap sampling methods were used to estimate the sampling distribution: the shift method was used for paired tests, and randomization was performed for two-sample tests [35].

Adding proprioception feedback to torque prediction

For the torque predictions, models were also created that used not only the neural discharge as inputs, but also the angular positions and velocities at a delay of *K* time steps:

$$\hat{\tau}_{1,j} = f_{1,0} + f_{1,\dot{\theta}_1}\dot{\theta}_{1,j-K} + f_{1,\dot{\theta}_2}\dot{\theta}_{2,j-K} + f_{1,\theta_1}\theta_{1,j-K} + f_{1,\theta_2}\theta_{2,j-K} + \sum_{n=1}^{N}\sum_{i=1}^{L} r_{j-i}^{n} f_{1,i}^{n} \text{ , and} \quad (5a)$$

$$\hat{\tau}_{2,j} = f_{2,0} + f_{2,\dot{\theta}_1}\dot{\theta}_{1,j-K} + f_{2,\dot{\theta}_2}\dot{\theta}_{2,j-K} + f_{2,\theta_1}\theta_{1,j-K} + f_{2,\theta_2}\theta_{2,j-K} + \sum_{n=1}^{N}\sum_{i=1}^{L} r_{j-i}^{n} f_{2,i}^{n} , \quad (5b)$$

where the notation "*j-K*" should be interpreted as the variable sampled at a delay of *K* units of time prior to the j^{th} time bin, and the additional subscripts (1 and 2) correspond to the shoulder and elbow joints, respectively. The joint position and velocity signals were filtered using a casual filter. As in the model of equation (3), the coefficients were estimated using the pseudo-inverse method. These additional terms can be interpreted in two ways: first, as a simple model of the visco-elastic properties of the musculoskeletal system, and second as a model of joint-related afferent feedback to the cortex. In either case, the intent was not to capture the full nonlinear and timing complexity of the system, but instead to explore the performance implications of having a small amount of additional information about the state of the arm in forming the predictive models.

Results

Although the monkey was given a wide variety of target positions to attain, the shoulder and elbow joint torques were significantly correlated (average R = 0.65 over all data sets, $p < 10^{-20}$, Fisher's R to Z transform and Z test; Cohen, 1995). This apparent synergy between the shoulder and elbow torques has been observed in human arm reaching as well [36, 37]. The mean peak correlation between the X and Y components of hand position was not substantial

($R = -0.04$). In addition, the highest magnitude correlation between hand position and torque was observed between Y and the shoulder, but this correlation was not substantial ($R = -0.3$). The mean peak correlations between torque and angular velocity of the corresponding joint and between torque and angular acceleration were 0.34 and 0.61, respectively.

Using the linear filter decoder, we were able to reconstruct both the position and the joint torque signals. Figure 2 shows examples of both from data set RS2 (N = 86 neurons). Panels a, b show the X and Y components of hand position. The corresponding shoulder and elbow torque predictions are shown in panels c, d. Although data were collected continuously, only successful trials were analyzed. Hence, the dashed lines indicate segments where discontinuous signals were concatenated for display purposes. The activity history of each neuron used in forming a prediction never crossed these discontinuities.

The higher frequency content of torque compared to position is evident in both the actual and the predicted signals. Prediction performance was assessed by computing the fraction of variance accounted for (FVAF) on test data that had not been used to build the model. In this example the accuracy of torque prediction was comparable to that of hand position. However, across the entire 2.4 minutes of this test data set, FVAF values were 0.76 and 0.67 for shoulder and elbow torques, respectively, versus 0.83 and 0.80 for the X and Y hand positions, respectively.

Figure 3 summarizes the average FVAF values across the six data sets. FVAF ranged from 0.19 to 0.87 for joint torque, 0.34 to 0.86 for Cartesian position, and 0.36 to 0.88 for Cartesian velocity. Shoulder torque was predicted more accurately than elbow torque (mean FVAF difference = 0.107, paired bootstrap test, $p < 10^{-6}$). There was no significant difference between the predictions of X and Y position and velocity ($p < .68$ and $p < .17$, respectively, paired bootstrap test). Over the six data sets and 20 folds, the Cartesian predictors outperformed the torque predictors by an average of 0.043 in the FVAF measure; this difference was significant according to a two-sample bootstrap test ($p < .002$). Cartesian velocity decoders performed on average better than both the Cartesian position and torque decoders by 0.033 and 0.077, respectively. These differences were significant according to a two-sample bootstrap test ($p < .01$ and $p < 10^{-6}$, respectively). The mean difference in FVAF values (over all six data sets) between training and test data was 0.03 and 0.04 for shoulder and elbow torque reconstructions, respectively, and 0.04 for both the X and Y components of the hand position; all differences

were significant according to a paired bootstrap test ($p < 10^{-6}$). This indicates the possibility of a small over-fitting effect, though not a serious one.

Proprioceptive feedback and torque prediction

In the intact nervous system, accurate motor control depends on multiple sources of sensory feedback, including proprioception via both fast spinal reflexes and slower long-loop reflexes mediated through the cortex [38]. We simulated the effect of proprioceptive feedback by including inputs to the torque decoder (right side of equations 5a and 5b) that corresponded to the joint angular positions and velocities at a fixed time prior to the torque prediction. In order to ensure that the trained decoder was realizable in an on-line control context, the proprioceptive feedback was filtered using a causal Butterworth filter. This filter induced delays in these signals on the order of 50 ms. We assessed the performance of these modified decoders using the validation data sets by varying the feedback time lag (K) from 0 to 1000 ms for data set RS2 (Figure 4a). Note that this feedback time lag is in addition to the delay induced by the filter. Decoding performance peaked at a delay of K=100 ms. For delays of 500 ms and greater, performance was comparable to having no proprioceptive feedback.

Over all six data sets across three animals, the torque decoding performance was significantly improved with the addition of proprioceptive feedback at a delay of K=100 ms (mean improvement was 0.168, $p < 10^{-6}$, paired bootstrap test; Figure 4b). The performance of the torque decoder with delayed feedback was significantly higher than both the Cartesian position and velocity decoders (mean difference in FVAF was 0.12 and 0.09, respectively; two-sample bootstrap test, $p < 10^{-6}$).

Temporal structure of decoders

As already discussed, the Cartesian position and joint torque signals have peak power at different frequencies. One question is whether these differences are reflected in the decoder coefficients. For a given filter lag, i, we computed the mean absolute filter coefficient, $\bar{f}_i$, across the set of neurons:

$$\bar{f}_i = \frac{1}{N}\sum_{n=1}^{N}\left| f_i^{\,n} \right|. \qquad (6)$$

This measure can be interpreted as the importance of time delay i to the prediction made by the decoder, relative to the other time delays. Figure 5 shows this measure as a function of delay for a representative experiment. Each curve corresponds to a single decoder type: Cartesian position, torque, and torque with proprioception. Because predictions by the different decoders are made in terms of different units, the absolute coefficient magnitude between decoders is arbitrary. The $\bar{f}_i$'s are therefore scaled so that the maximum for a given decoder is unity.

Figure 5 shows that the Cartesian position decoder placed a majority of weight on cell activity in the first 450 ms, but also included substantial weight over the entire one second. In contrast, the torque decoders primarily incorporated information from the first 200-300 ms. This difference between the Cartesian position and torque decoders was consistent across the six data sets. This distinction may be due to the differences in the component frequencies contained within the two classes of predictions: because of its lower bandwidth, Cartesian position does not change as quickly, the decoder can average information from a longer history of neural signals. In contrast, the higher frequency content of the torque signals implies that only the recent history of the neural signals contains information relevant to the current prediction.

Figure 5 also shows a distinction between the torque and the torque-with-proprioception decoders; this distinction was clear in half of the data sets. In particular, the torque decoder placed more emphasis on the 200-450 ms time range than did the modified decoder. As discussed above, substantial position information is present in the first 450 ms of neural data before movement. However, when joint position and velocity are explicitly available to the decoder from the feedback terms, the only information that must be extracted from the history of cell activity is the intended acceleration. Because the acceleration signals have peak power at higher frequencies than position, the decoder will focus on the information that is available just prior to the predicted movement.

Stability of learned decoders

Ultimately, we are interested in the development of decoders for chronic use; one key question is the stability of a decoder over time. We examined this question by constructing a set of decoders using training data derived from the first half of an experimental session, and then comparing the performance on the trials from the third and fourth quarters of the session. As in the previous experiments, data set RS2 was partitioned into 20 data folds, each containing equal numbers of trials. The first ten folds were used to construct ten different decoders of both

Cartesian position and torque (each model used nine of the ten available training folds). The performance of each decoder was tested using folds 11-15 (early) and 16-20 (late). The difference in torque performance was not significant ($p < 0.4$, paired bootstrap test). The mean performance of the Cartesian position decoder was 0.01 higher in FVAF for the "late" data set ($p < 6 \times 10^{-4}$, paired bootstrap test). This result suggests that the learned decoders are stable over the duration of the experimental session (90 minutes for the case of data set RS2).

Discussion

We have shown that neural activity from ensembles of simultaneously recorded neurons in the primary motor cortex can be used to reconstruct time-varying joint torques at the shoulder and elbow during constrained movements of the arm in the horizontal plane. To our knowledge, this is the first demonstration of kinetic decoding of proximal arm movements. The accuracy of reconstructions of shoulder and elbow joint torque was nearly equivalent to that of Cartesian hand position and slightly less than that of Cartesian velocity. This study is intended as a demonstration of the feasibility of extracting kinetic information from MI for use in controlling a dynamic limb. Because of the significant remaining correlations between joint torque and movement kinematics, it is impossible to make strong assertions about whether either set of signals represents the fundamental signals "encoded" by MI. Nonetheless, it is quite possible that a BMI-controlled prosthetic device that would both move and exert contact force, would benefit from the use of kinetic control signals, either alone or in combination with kinematic signals.

Proprioceptive feedback

We have also demonstrated that the addition of limb-state information to the torque decoder resulted in significant improvements in decoding accuracy. The joint position and velocity were filtered using a causal filter, which induces a signal delay but affords a real-time implementation. These very simple simulations of linear proprioceptive feedback suggest that a practical BMI for use in spinal injured patients would benefit from the introduction of artificial sensory signals to the controller that include the state of the controlled device. It should be emphasized that the sensory signals we simulated were fed back to the decoder and not to the animal.

The randomly-placed targets used in this study allowed movements to be significantly less constrained than are the movements to a limited number of fixed targets. However, there remained significant linear correlations between joint angular position/velocity and torque. If these signals were further decoupled, the benefit of this simple linear feedback would certainly be reduced. Incorporation of nonlinear feedback signals should also be considered.

Technical issues and potential improvements

In our analysis, we have followed [30] in using a "fraction of variance accounted for" measure of performance as opposed to the R-squared measure. FVAF is stricter in that it requires a perfect match between the prediction and the observation, rather than a simple correlation. This distinction is particularly important once one begins to use these predictions to drive the motion of a prosthetic or robotic arm. Furthermore, the computation of the R-squared statistic involves a linear regression step that makes use of the test data set to select optimal gain and offset parameters. Because the training data are being used in the selection of model parameters, the data set is not independent of the training process. Hence, a significant bias can be introduced into the evaluation process that can mask the utility of the resulting predictors in novel/independent contexts, such as when controlling a prosthetic arm.

In practice, the pseudo-inverse solution to this form of linear filter decoder can be unstable when training set sizes are small and/or the number of recorded cells is large. We are exploring the use of a modified form of the pseudo-inverse method that includes a smoothness term in the error function. This method addresses the function over-fitting issues that can arise in these unstable situations, leading in some cases to dramatic improvements in performance.

Relation between kinematic and kinetic parameters

At first glance, it is perhaps not surprising that the accuracy of joint torque reconstruction is similar to that of hand position and velocity, given their relationship through the equations of motion and arm kinematics. However, it should be emphasized that joint torque represents a much richer signal, as is evident from its significantly larger bandwidth. Therefore, it is not obvious *a priori* that the torque decoding performance would have been comparable to that of hand position. It is possible that the slightly higher frequency content of the elbow torque signals may have been a factor in the lower prediction quality of elbow torque compared to that of the shoulder. Because of the strong correlations between joint torque and both angular

velocity and acceleration, we cannot address the long-standing controversy as to whether MI codes primarily for kinetic versus kinematic parameters of movement. However, our primary aim in this study was to determine whether kinetic decoding is possible for brain-machine interface applications, comparable to results from previous studies that have decoded position and velocity.

Our results are consistent with the observations of other groups that have studied single neurons and found significant correlations with both kinetic as well as kinematic signals [6, 39-41]. There is some evidence that the most caudal area of MI within the bank of the central sulcus may be more be directly related to muscle activity and the dynamics of movement, as compared to the precentral gyrus where our recordings were made [42]. Therefore, torque decoding may be even more accurate if it could be based on motor cortical populations within the bank of the central sulcus.

Implications for brain-machine interface development

It would be of great interest to determine a monkey's ability to use kinetic signals for real-time, closed-loop control. Such a control system might provide greater ability to generalize control across a variety of dynamical conditions and external loading. One potential concern with kinetic control is that small torque prediction errors, when applied open loop to a forward dynamics limb model will lead to significant position error. Our analyses suggest that it takes at least 400 ms for a substantial error to accumulate. This degree of drift is unlikely to be problematic in the closed-loop context, as the subject could correct for any significant position error via visual feedback. This situation is not unlike the significant improvement that was realized for position control when the brain-control loop was first closed. Initial estimates (based on open-loop studies) of the number of neurons that would be required to achieve adequate control ranged into the hundreds of neurons [14]. However, when monkey subjects were given the ability to correct position decoding errors, control was achieved with only 10s of neurons [15, 16].

Table 1: Data set sizes

Data Set	Number of Cells
RJ1	48
RJ2	61
BO1	36
BO2	31
RS1	99
RS2	86

Appendix A: Determination of Parameter Values

Definitions and values of quantities used in Equations (1) and (2) are given in Table 2. Note that only inter-joint lengths (L_1 and L_3) appear directly in Equations (1) and (2), because they contribute to the effective inertia components for segments 2 and 4, respectively. L_2 and L_4 thus do not directly enter the equations, although L_2 is employed in the kinematics equations relating Cartesian position of the KINARM handle to angular coordinates.

Rotational inertias for all components of the monkey/KINARM system were computed with respect to their proximal pivots, by the addition of products of their masses with squared distances between pivots and centers of mass of each component. In computing inertias of animal and KINARM segments, the hand was treated as a point mass at the location of the palm, and forearm troughs and rests were treated as linear masses located at their centers. The upper arm was treated as a uniform on-axis cylinder.

Table 2: KINARM and monkey mechanical properties

Term	**Definition**	**RJ1,RJ2**	**B1,B2**	**RS1,RS2**
M_1	Total mass of segment 1 (g): M_{1K}+ M_{1A}	919	947	1390
M_2	Total mass of segment 2 (g): M_{2K}+ M_{2A}	636	656	801
M_{1K}	Mass of KINARM segment 1[a] (g)	635	635	1040.
M_{2K}	Mass of KINARM segments 2+5[a](g)	391	391	509
M_{1A}	Upper arm mass of animal[b](g)	284	312	350.
M_{2A}	Forearm mass of animal[b](includes hand) (g)	244	265	292.
M_3	Mass of KINARM segment 3(g)	637	637	978.
M_4	Mass of KINARM segment 4(g)	117	117	162.
M_{hand}	Hand mass of animal[b](g)	56	59	62.
$M_{forearm}$	Forearm mass of animal[b] (excludes hand) (g)	188	206	230.
M_A	Total animal mass (kg)	7.6	8.4	9.50
I_{1K}	Rotational inertia of KINARM segment 1[c](gcm^2)	$2.64x10^4$	$2.64x10^4$	$4.30x10^4$
I_{2K} + I_{5K}	Rotational inertia of KINARM segment 2+5[c](gcm^2)	$4.39x10^4$	$4.66x10^4$	$5.49x10^4$
I_{1A}	Rotational inertia of animal upper arm[d](gcm^2)	$4.51x10^4$	$5.72x10^4$	$4.68x10^4$
I_{2A}	Rotational inertia of animal forearm[d](gcm^2)	$3.48x10^4$	$4.31x10^4$	$3.47x10^4$
I_1	Total rotational inertia of segment 1	I_{1K} + I_{1A}		
I_2	Total rotational inertia of segment 2	I_{2K} + I_{2A}		
I_3	Rotational inertia of KINARM segment 3[c](gcm^2)	$1.84x10^4$	$1.84x10^4$	$6.38x10^4$
I_4	Rotational inertia of segment 4 [c] (gcm^2)	$1.76x10^4$	$1.76x10^4$	$9.00x10^3$
$I_{M1,}$ I_{M2}	Rotational inertias of torque motors (gcm^2)	7920.	7920.	7920.
L_1	Length of segment #1 and monkey upper arm (cm)[e]	13.9	15.0	13.0
L_2	Length of segment #2 and monkey forearm (to palm of hand, cm)[e]	20.4	22.0	19.0
L_3	Inter-joint length (cm)	6.7	6.7	6.7
l_{radius}	Animal radius bone length [e] (cm)	15.5	17.2	14.3
$\overline{X}_{1K}, \overline{Y}_{1K}$	Center of mass coordinates of KINARM segment 1 (cm).	3.24,-0.83	3.24,-0.83	2.22,-3.44
$\overline{X}_{2K}, \overline{Y}_{2K}$	Center of mass coordinate of KINARM segment 2 (cm).	2.75,-0.83	2.75,-0.83	0.49,-1.31
$\overline{X}_{3K}, \overline{Y}_{3K}$	Center of mass coordinate of KINARM segment 3 (cm).	3.31, 0	3.31, 0	5.52, 0
$\overline{X}_{4K}, \overline{Y}_{4K}$	Center of mass coordinate of KINARM segment 4 (cm).	10.06, 0	10.06, 0	4.65, 0
$\overline{X}_{1A}, \overline{Y}_{1A}$	Center of mass coordinates of monkey upper arm[f](cm)	6.95, 0	7.50, 0	6.5, 0
$\overline{X}_{2A}, \overline{Y}_{2A}$	Center of mass coordinates of monkey forearm[g](cm)	9.93, 0	10.83, 0	8.98, 0

a M_{1k} includes arm rest, and M_{2k} includes forearm rest, forearm trough, and handle-grip.

b Masses M_{1A} , M_{2A} , M_{hand} , $M_{forearm}$ were computed from the linear regressions described by Cheng and Scott (2000) (table 8) based on total animal mass $M_{A.}$

c KINARM segment inertias were obtained from Ian Brown (personal communication) and subsequently modified for rotation about proximal pivots, rather than centers of mass, using the parallel axis theorem. This requires the use of the Xikbar, Yikbar values quoted in the table. Inertias of arm troughs, rests, and KINARM handle were added to give total inertias of segments 1 and 2.

d Animal arm inertias were calculated from the regression formulae of Cheng and Scott (2000), modified for rotation about proximal pivots, rather than centers of mass.

e Lengths of upper arm, forearm (to palm of hand), and radius were determined from x-ray images of each monkey.

f Upper arm was treated as a uniform circular cylinder.

g Forearm center of mass (without hand) was assumed to be $0.44l_{radius}$ (Cheng & Scott, 2000). Hand was treated as a point mass at position of palm (distance $l2$ from elbow joint).

Acknowledgements We thank Matthew Fellows, Elise Gunderson, Zach Haga, Dawn Paulsen, and Jake Reimer for their help with the surgical implantation of the arrays, training of monkeys, and data collection. Inertial properties of segments of the KINARM were supplied by Ian Brown. We also thank David Goldberg for his assistance in conducting and analyzing the decoding experiments.

Competing interests statement Nicholas Hatsopoulos has stock ownership in a company, Cyberkinetics Neurotechnology Systems, Inc. that fabricates and sells the multi-electrode arrays and acquisition system used in this study.

Figure legends

Figure 1. Illustration of the monkey's arm configuration on the exoskeletal robot (KINARM). Joint angular positions, θ_1 and θ_2, were sampled directly. Cartesian position of the hand *(X,Y)* was calculated using the joint angles and arm segment lengths, L_1 and L_2.

Figure 2. Decoding of Cartesian position (**a** and **b**) and joint torque (**c** and **d**). Thick red lines indicate actual position or torque, while the thin blue lines indicate the predicted signals estimated from the model. The gray areas represent the 95% *prediction region* for each quantity. The dashed vertical lines represent trial boundaries.

Figure 3. Summary of decoding results. Mean fraction of variance accounted for (FVAF) by the decoding models, for Cartesian position (squares), Cartesian velocity (circles), and joint torque (diamonds). Markers indicate mean FAVF over 20 cross-validated folds. Error bars represent standard deviations over the 20 cross-validated folds.

Figure 4. Joint torque FVAF with the addition of simulated proprioceptive feedback. **a**. FVAF as a function of the time delay between spike discharge and feedback (including a no feedback condition) for data set RS2. **b**. FVAF for all six data sets with (white) and without (black) feedback using the delay of 100 ms.

Figure 5. Scaled mean absolute filter coefficient as a function of delay between filter time bin and arm state prediction. Each curve corresponds to a different decoder: Cartesian position (dashed line), torque (solid, thin), and torque with proprioception (solid, thick). Mean is computed over all cells from a single decoder.

References

[1] **E. V. Evarts, "Relation of pyramidal tract activity to force exerted during voluntary movement," *Journal of Neurophysiology*, vol. 31, pp. 14-27, 1968.**

[2] **A. P. Georgopoulos, J. F. Kalaska, R. Caminiti, and J. T. Massey, "On the relations between the direction of two-dimensional arm movements and cell discharge in primate motor cortex," vol. 2, pp. 1527-1537, 1982.**

[3] **A. M. Smith, M. C. Hepp-Reymond, and U. R. Wyss, "Relation of activity in precentral cortical neurons to force and rate of force change during isometric contractions of finger muscles," *Exp Brain Res*, vol. 23, pp. 315-32, 1975.**

[4] **M.-C. Hepp-Reymond, U. R. Wyss, and R. Anner, "Neuronal coding of static force in the primate motor cortex," vol. 74, pp. 287-291, 1978.**

[5] **P. D. Cheney and E. E. Fetz, "Functional classes of primate corticomotoneuronal cells and their relation to active force," *J Neurophysiol*, vol. 44, pp. 773-91, 1980.**

[6] **J. F. Kalaska, D. A. D. Cohen, M. L. Hyde, and M. Prud'homme, "A comparison of movement direction-related versus load direction-related activity in primate motor cortex, using a two-dimensional reaching task," vol. 9, pp. 2080-2102, 1989.**

[7] **M. Taira, J. Boline, N. Smyrnis, A. P. Georgopoulos, and J. Ashe, "On the relations between single cell activity in the motor cortex and the direction and magnitude of three-dimensional static isometric force," *Exp Brain Res*, vol. 109, pp. 367-76, 1996.**

[8] **D. W. Cabel, P. Cisek, and S. H. Scott, "Neural activity in primary motor cortex related to mechanical loads applied to the shoulder and elbow during a postural task," *J Neurophysiol*, vol. 86, pp. 2102-8, 2001.**

[9] **L. E. Sergio, C. Hamel-Paquet, and J. F. Kalaska, "Motor cortex neural correlates of output kinematics and kinetics during isometric-force and arm-reaching tasks," *J Neurophysiol*, vol. 94, pp. 2353-78, 2005.**

[10] **A. P. Georgopoulos, R. Caminiti, and J. F. Kalaska, "Static spatial effects in motor cortex and area 5: Quantitative relations in a two-dimensional space," *Experimental Brain Research*, vol. 54, pp. 446-454, 1984.**

[11] **L. Paninski, M. R. Fellows, N. G. Hatsopoulos, and J. P. Donoghue, "Spatiotemporal tuning of motor cortical neurons for hand position and velocity," *Journal of Neurophysiology*, vol. 91, pp. 515-532, 2004.**

[12] **D. W. Moran and A. B. Schwartz, "Motor cortical representation of speed and direction during reaching," *J Neurophysiol*, vol. 82, pp. 2676-92, 1999.**

[13] **D. W. Moran and A. B. Schwartz, "Motor cortical activity during drawing movements: population representation during spiral tracing," *J Neurophysiol*, vol. 82, pp. 2693-704, 1999.**

[14] **J. Wessberg, C. R. Stambaugh, J. D. Kralik, P. D. Beck, M. Laubach, J. K. Chapin, J. Kim, S. J. Biggs, M. A. Srinivasan, and M. A. Nicolelis, "Real-time prediction of hand trajectory by ensembles of cortical neurons in primates," *Nature*, vol. 408, pp. 361-5, 2000.**

[15] **M. D. Serruya, N. G. Hatsopoulos, L. Paninski, M. R. Fellows, and J. P. Donoghue, "Instant neural control of a movement signal," *Nature*, vol. 416, pp. 141-2, 2002.**

[16] **D. M. Taylor, S. I. Tillery, and A. B. Schwartz, "Direct cortical control of 3D neuroprosthetic devices," *Science*, vol. 296, pp. 1829-32, 2002.**

[17] **J. R. Wolpaw and D. J. McFarland, "Control of a two-dimensional movement signal by a noninvasive brain-computer interface in humans," *Proc Natl Acad Sci U S A*, vol. 101, pp. 17849-54, 2004.**

[18] **D. R. Humphrey, E. M. Schmidt, and W. D. Thompson, "Predicting measures of motor performance from multiple cortical spike trains," *Science*, vol. 170, pp. 758-62, 1970.**

[19] **J. M. Carmena, M. A. Lebedev, R. E. Crist, J. E. O'Doherty, D. M. Santucci, D. F. Dimitrov, P. G. Patil, C. S. Henriquez, and M. A. Nicolelis, "Learning to control a brain-machine interface for reaching and grasping by primates," *Public Library of Science, Biology*, vol. 1, pp. 1-16, 2003.**

[20] **M. M. Morrow and L. E. Miller, "Prediction of muscle activity by populations of sequentially recorded primary motor cortex neurons," *J Neurophysiol*, vol. 89, pp. 2279-88, 2003.**

[21] **D. M. Santucci, J. D. Kralik, M. A. Lebedev, and M. A. Nicolelis, "Frontal and parietal cortical ensembles predict single-trial muscle activity during reaching movements in primates," *Eur J Neurosci*, vol. 22, pp. 1529-40, 2005.**

[22] **D. T. Westwick, E. A. Pohlmeyer, S. A. Solla, L. E. Miller, and E. J. Perreault, "Identification of multiple-input systems with highly coupled inputs: application to EMG prediction from multiple intracortical electrodes," *Neural Comput*, vol. 18, pp. 329-55, 2006.**

[23] **E. A. Pohlmeyer, S. A. Solla, E. J. Perreault, and L. E. Miller, "Prediction of upper limb muscle activity from motor cortical discharge during reaching," *J Neural Eng*, vol. 4, pp. 369-79, 2007.**

[24] **S. H. Scott, "Apparatus for measuring and perturbing shoulder and elbow joint positions and torques during reaching," *J Neurosci Methods*, vol. 89, pp. 119-27, 1999.**

[25] **J. M. Hollerbach and T. Flash, "Dynamic interactions between limb segments during planar arm movement," *Biological Cyberkinetics*, vol. 44, pp. 67-77, 1982.**

[26] **E. J. Cheng and S. H. Scott, "Morphometry of Macaca mulatta Forelimb. I. Shoulder and Elbow Muscles and Segment Inertial Parameters," *Journal of Morphology*, vol. 245, pp. 206-224, 2000.**

[27] **H. Goldstein, *Classical Mechanics*. Reading, Massachusetts: Addison-Wesley Publishing Co., 1959.**

[28] **A. V. Oppenheim and R. W. Shafer, *Discrete-Time Signal Processing*. Englewood Cliffs, New Jersey: Prentice-Hall, 1989.**

[29] **R. Penrose, "A generalized inverse for matrices," *Proceedings of the Cambridge Philosophical Society*, vol. 51, pp. 406-413, 1955.**

[30] **M. Serruya, N. Hatsopoulos, M. Fellows, L. Paninski, and J. Donoghue, "Robustness of neuroprosthetic decoding algorithms," *Biol Cybern*, vol. 88, pp. 219-28, 2003.**

[31] **M. Stone, "Cross-validatory choice and assessment of statistical predictions," *Journal of the Royal Statistical Society Series B-Methodological*, vol. 36, pp. 111-147, 1974.**

[32] **C. Bishop, *Neural networks for pattern recognition*. Oxford: Oxford University Press, 1996.**

[33] **M. W. Browne, "Cross-validation methods," *Journal of Mathematical Psychology*, vol. 44, pp. 108-132, 2000.**

[34] **S. S. Shapiro and M. B. Wilk, "An analysis of variance test for normality (complete samples)," *Biometrika*, vol. 52, pp. 591-611, 1965.**

[35] **P. R. Cohen, *Empirical Methods for Computer Science*. Cambridge, MA: MIT Press, 1995.**

[36] **G. L. Gottlieb, Q. Song, D. A. Hong, G. L. Almeida, and D. Corcos, "Coordinating movement at two joints: a principle of linear covariance," *J Neurophysiol*, vol. 75, pp. 1760-4, 1996.**

[37] **G. L. Gottlieb, Q. Song, D. A. Hong, and D. M. Corcos, "Coordinating two degrees of freedom during human arm movement: load and speed invariance of relative joint torques," *J Neurophysiol*, vol. 76, pp. 3196-206, 1996.**

[38] **P. D. Cheney and E. E. Fetz, "Corticomotoneuronal cells contribute to long-latency stretch reflexes in the rhesus monkey," *J Physiol*, vol. 349, pp. 249-72, 1984.**

[39] **W. T. Thach, "Correlation of neural discharge with pattern and force of muscular activity, joint position, and direction of intended next movement in motor cortex and cerebellum," *J. Neurophysiol.*, vol. 41, pp. 654-676, 1978.**

[40] **S. Kakei, D. S. Hoffman, and P. L. Strick, "Muscle and Movement Representations in the Primary Motor Cortex," *Science*, vol. 285, pp. 2136-2139, 1999.**

[41] **S. Kakei, D. S. Hoffman, and P. L. Strick, "Direction of action is represented in the ventral premotor cortex," *Nat Neurosci*, vol. 4, pp. 1020-5, 2001.**

[42] **J. A. Rathelot and P. L. Strick, "Muscle representation in the macaque motor cortex: an anatomical perspective," *Proc Natl Acad Sci U S A*, vol. 103, pp. 8257-62, 2006.**

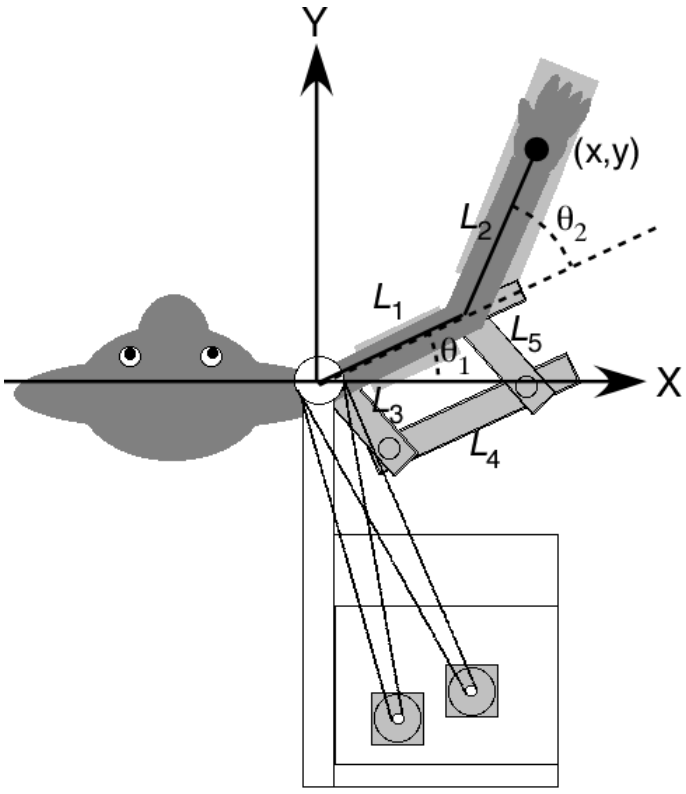

Figure 1

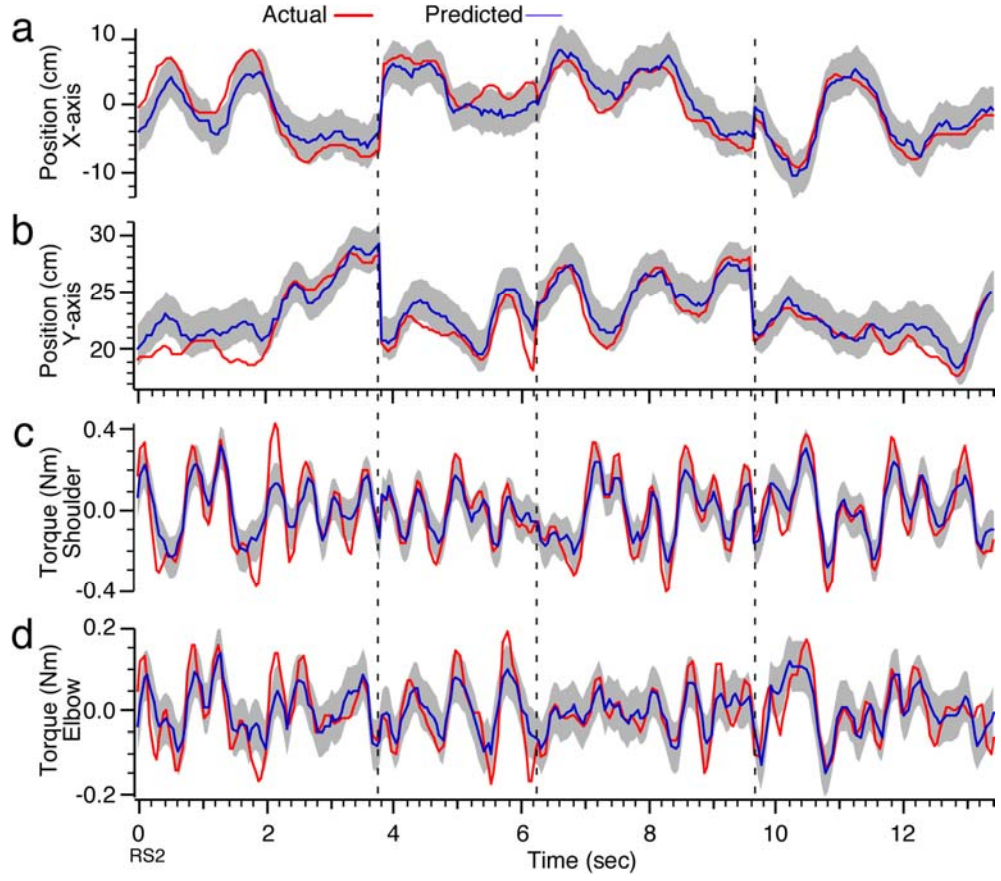
Actual
Predicted
a
Position (cm)
X-axis
10
0
-10
b
Position (cm)
Y-axis
30
25
20
c
Torque (Nm)
Shoulder
0.4
0.0
-0.4
d
Torque (Nm)
Elbow
0.2
0.0
-0.2
0
RS2
2
4
6
8
10
12
Time (sec)

Figure 2

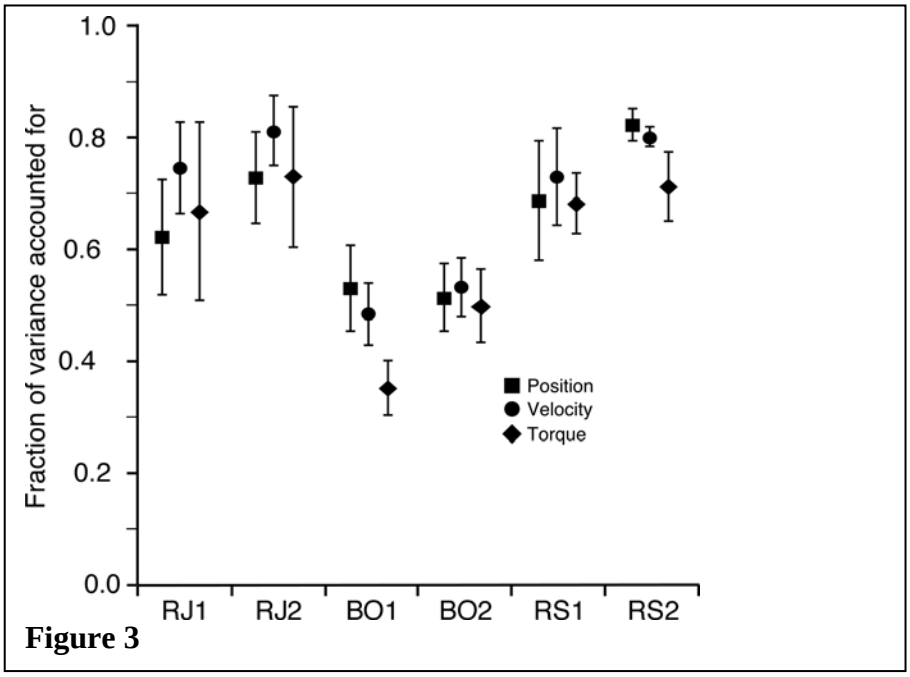
1.0
0.8
0.6
0.4
0.2
0.0
Fraction of variance accounted for
RJ1
RJ2
BO1
BO2
RS1
RS2
Position
Velocity
Torque

Figure 3

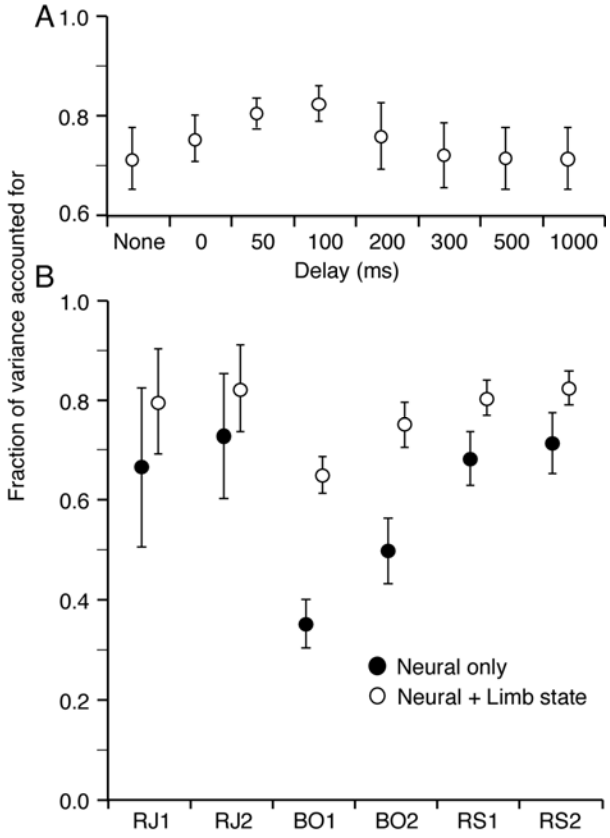
A
1.0
0.8
0.6
None
0
50
100
200
300
500
1000
Delay (ms)
B
Fraction of variance accounted for
1.0
0.8
0.6
0.4
0.2
0.0
RJ1
RJ2
BO1
BO2
RS1
RS2
Neural only
Neural + Limb state

Figure 4

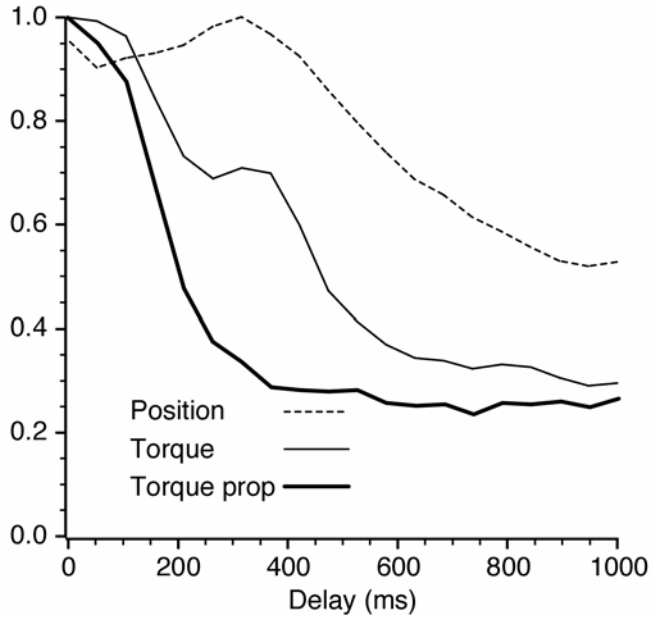
1.0
0.8
0.6
0.4
0.2
0.0
0
200
400
600
800
1000
Delay (ms)
Position
Torque
Torque prop

Figure 5